Bioconjugate Chemistry

Article

pubs.acs.org/bc

Click Chemistry Approach for Imaging Intracellular and Intratissue Distribution of Curcumin and Its Nanoscale Carrier

Zhen Luo,[†] Rohan V. Tikekar,[‡,§] and Nitin Nitin*[,†,‡]

[†]Department of Biological Engineering and [‡]Department of Food Science and Technology, University of California-Davis, Davis, California 95616, United States

[§]Program in Food Science, Drexel University, Philadelphia, Pennsylvania 19104, United States

Supporting Information

ABSTRACT: This study was aimed at developing a fluorescence imaging approach to simultaneously characterize the delivery and distribution of a bioactive molecule, curcumin, and its micelle based nanoscale carrier in cells and tissue models. To enable imaging of curcumin, a monoalkyne derivative of curcumin was synthesized and purified using LC-MS. Intracellular uptake of curcumin was characterized using a click chemistry reaction between a monoalkyne modified curcumin and Alexa-488 azide fluorescent dye in cells and tissues. Fluorescence images of cells and tissues incubated with monoalkyne curcumin showed specific detection of intracellular delivered monoalkyne curcumin using the click chemistry reaction. The fluorescence imaging results also demonstrated significant improvement in detection sensitivity of intracellular delivered curcumin as compared to measurements based on native fluorescence of unmodified curcumin. Intracellular uptake of monoalkyne curcumin was characterized as a function of incubation time and concentration. The results show a rapid uptake of monoalkyne curcumin during the first 4 h of incubation. Modification of curcumin to its monoalkyne derivative did not impact its apoptotic activity in cancer cells. DSPE-PEG micelles labeled with Alexa-647 were selected as a representative nanoscale carrier to enhance the solubility and delivery of monoalkyne curcumin. Fluorescence images of cells and tissues incubated with fluorescently labeled micelles containing monoalkyne curcumin clearly illustrate significant differences in intracellular and intratissue localization of DSPE-PEG and encapsulated monoalkyne curcumin. The imaging approach developed in this study can be used to understand delivery and distribution of diverse bioactive compounds and their nanocarrier systems as well as in situ measurement of interactions of bioactives with cellular and tissue targets.

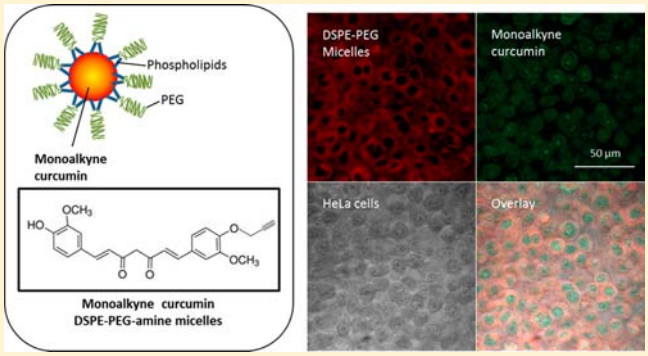

INTRODUCTION

Plant derived small bioactive molecules such as polyphenols, flavones, and isoflavones have potential to reduce inflammation, and both prevent and treat diverse chronic diseases such as cancer and neurodegenerative diseases.[1−5] Despite its significant potential, there is limited understanding of the interactions of these bioactives with diverse cellular targets. One of the factors that limit this understanding is the lack of in situ imaging approaches to characterize intracellular and intratissue distribution of these bioactives. Furthermore, many of these small bioactive molecules have poor solubility in aqueous medium and consequently exhibit limited bioavailability.[6−8] Significant efforts have been made to encapsulate these bioactives in diverse colloidal carriers to improve stability and solubility in aqueous environment and to enhance the delivery of these bioactives to cells and tissues.[6−9] However, fate of these self-assembled colloidal carriers and their encapsulants in cells and tissue environment is not well characterized. In situ imaging approaches to simultaneously measure intracellular and intratissue distribution of self-assembled colloid carriers and encapsulated bioactives can enable characterization of the fate of colloidal carriers and their encapsulants in cellular and tissue environments and guide development of novel delivery systems.

Delivery of small molecular weight bioactive compounds in cells and tissue has been predominantly characterized using chemical analysis (such as LC-MS) of cellular and tissue lysates. Using the chemical analysis approach, both the bioactives and their metabolites are measured to quantify the total amount of bioactives delivered to cells and tissue.[10−12] Chemical analysis of cell and tissue lysates can quantify the total amount of bioactive compounds delivered to cells and tissue but cannot map spatial variations in cellular and tissue distribution of bioactives. Furthermore, in situ monitoring of interactions of small molecular weight bioactive compounds with target molecules in cells and tissues cannot be assessed. To

Received: April 18, 2013
Revised: December 11, 2013
Published: December 14, 2013

complement the chemical analysis of tissue lysates, efforts have been made to image the distribution of some small molecules such as curcumin based on native fluorescence properties of small bioactive molecules.[13,14] However, due to a significant overlap of curcumin fluorescence spectrum with native cellular autofluorescence and its limited fluorescence quantum yield,[13] the sensitivity and specificity of this approach is limited. The problem of imaging curcumin based on its fluorescence properties is further exacerbated in tissues due to significantly higher levels of autofluorescence in 3-d tissues compared to individual cells in a 2-d cell culture model.[15,16] To address these limitations, a covalent modification of small molecules with exogenous fluorophores prior to delivery has been considered.[17] However, the results of prior studies have shown that conjugation of small molecules (MW < 500 Da) to conventional fluorescent dyes such as Alexa dyes (MW ranging between 700 and 1000 Da) significantly impact the distribution and biological activity of the small molecules.[17] Therefore, this approach is not typically used for imaging intracellular and intratissue distribution of small molecules.

In addition to optical imaging approaches, biodistribution of small molecules can also be imaged using positron emission tomography (PET). In this approach, small molecules such as curcumin have been modified with a radiotracer probe.[18,19] However, due to the limited spatial resolution of the PET imaging, high resolution mapping of the distribution of small molecules within cells and localized tissues cannot be achieved.[20] Thus, there is a need to develop molecular tagging approaches that can be used to specifically detect small bioactive molecules in cells and tissues without significantly influencing the chemical structure and biological activity of the selected molecules.

The objective of this study was to develop a novel optical molecular imaging approach to simultaneously characterize the delivery and distribution of a bioactive compound and its micelle based nanoscale carrier in cells and tissue models. Curcumin was selected as a model small bioactive molecule based on its clinical potential and its physical and chemical properties that are similar to a large class of polyphenols.[21−23] The novel imaging approach is based on development of a monoalkyne derivative of curcumin. A relatively small monoalkyne tag is stable in cells and tissue environment[24−26] and can be detected in situ using the click chemistry approach. In contrast to a conventional approach of labeling the molecule with a fluorescent dye before delivery, monoalkyne curcumin can be chemically conjugated to an azide modified fluorophore after its delivery in cells and tissues using click chemistry.

Phospholipid-PEG (polyethylene glycol) micelle was selected as a model nanocarrier system for this study, as prior research studies have shown improvement in the delivery of curcumin to cells and tissues using encapsulation systems as colloidal nanocarriers.[27,28] Furthermore, due to the unique size of micelles, these nanoscale carriers can be delivered through diverse delivery routes including oral, topical, and intravenous delivery.[29−32] Although these colloidal carriers are widely used for delivery of diverse bioactive molecules, there is limited understanding regarding the fate of encapsulation carrier and the bioactive molecules in cellular and tissue environment. Prior studies have shown that colloidal carriers and encapsulated small molecular weight fluorescent dyes can have significantly different localization in physiological environments including serum.[33,34] These differences in the localization of the carriers and the encapsulants may result due to significant changes in the structure and stability of nano- and microscale carriers upon interaction with physiological environments in cells and tissues.[33,34] To the best of our knowledge, none of the prior studies have demonstrated simultaneous imaging of the encapsulated bioactives and the nanoscale colloidal carriers in cell and tissue models. The significance of imaging distribution of bioactive molecules is based on the fact that these bioactives molecules have specific affinities for diverse class of biomolecules in cells and tissues that can significantly influence their partitioning in subcellular and tissue domains. Thus, direct and simultaneous measurement of the distribution of bioactive small molecules and its nano- or microscale carriers in cells and tissues is critical for improving the design of colloidal carriers. In this study, phospholipid-PEG micelles were prelabeled with a fluorescent dye before delivery to enable simultaneous imaging of nanoscale carriers and monoalkyne curcumin in cells and tissues.

In summary, the study develops a novel application of the click chemistry approach to map intracellular and intratissue distribution of small bioactive molecules. The results also provide a novel approach for simultaneous imaging of both the nanoscale carriers and the encapsulated molecules in model systems. These measurements in combination with biochemical assays are expected to have significant impact on comprehensive understanding of bioavailability and activity of these molecules in physiological environments.

MATERIALS AND METHODS

Materials. Curcumin, potassium carbonate, propargyl bromide, dimethyl formamide (DMF), methanol, dimethyl sulfoxide (DMSO), acetonitrile, copper sulfate, phosphate buffer saline (PBS), and ascorbic acid were obtained from Sigma-Aldrich Inc. (St. Louis, MO). DSPE-PEG-amine (1,2-distearoyl-*sn*-glycero-3-phosphoethanolamine-*N*-[amino-(polyethylene glycol)-2000]) was obtained from Avanti Polar Lipids Inc. (Alabaster, AL). Alexa-488 azide and NHS-azide were procured from Invitrogen (Grand Island, NY). C-18 solid phase columns were used for purification of crude reaction mixture prior to HPLC purification and Zeba Spin Desalting Column (7000 Da MWCO, Thermo, Rockford, IL) were used for removal of free fluorescent dye molecules after chemical conjugation. LC-MS (liquid chromatography−mass spectrometry) grade acetonitrile and isopropyl alcohol was purchased from Burdick and Jackson (VWR International, West Chester, PA). The ultrapure water was obtained from an in-house Millipore water purification system (Billerica, MA).

The human cervical carcinoma cell line (HeLa) was a gift from Professor Glenn M. Young (University of California, Davis). Dulbecco's modified Eagle's medium (DMEM), fetal bovine serum (FBS), trypsin, and trypan blue were obtained from Fisher Scientific (Pittsburgh, PA). Penicillin−streptomycin was purchased from Sigma-Aldrich, Inc. (St. Louis, MO). Type I collagen from rat tail was obtained from Roche, Inc. (South San Francisco, CA).

Monoalkyne Curcumin Synthesis. Monoalkyne curcumin synthesis was adapted based on the previously published method.[35] Briefly, 0.5 g (1.35 mmol) of curcumin was mixed with 0.94 g (6.8 mmol) of potassium carbonate and 0.81 g (6.8 mmol) propargyl bromide in 20 mL of DMF and incubated at 25 °C for 48 h under nitrogen with continuous stirring. Ten milliliters of distilled water was added to the mixture after 48 h and preliminary separation of reactants from products was carried out using C-18 solid phase extraction columns.

dx.doi.org/10.1021/bc4002008 | *Bioconjugate Chem.* 2014, 25, 32−42

Columns were activated by washing with 2 mL of water followed by 2 mL of methanol. The final wash was given with 2 mL of water before loading the crude mixture of product and reactants. Two milliliters of the reaction mixture was added to the column and eluted with 2 mL methanol. The methanolic extract was dried using a centrifuge evaporator at 50−60 °C for 2 h to remove traces of propargyl bromide. Adequacy of the evaporation process was confirmed by complete evaporation of control propargyl bromide solution prepared in methanol under identical experimental conditions. The dried sample was reconstituted in methanol.

Purification of Monoalkyne Curcumin. Purification of monoalkyne curcumin from the mixture was performed using a Surveyor HPLC separation module (ThermoFischer, San Jose, CA) coupled to LTQ linear ion trap MS (ThermoFinnigan, San Jose, CA). Onyx Monolithic Semi-PREP C18 columns were used for analytical (100 × 3 mm) and preparative (100 × 10 mm) runs with a C18 precolumn (Phenomenex Chromolith Guard Cartridge, RP-18e 10 × 4.6 mm). Injection volumes for analytical and preparative runs were 10 and 100 μL, respectively. The mobile phases were: A, 0.5% acetic acid in water; and B, pure acetonitrile. Column temperature was 35 °C and the flow rate was 4 mL/min. Run was operated under isocratic condition with 80% A and 20% B for 1 min after which a linear gradient was used to change the mobile composition to 100% B in next 9 min followed by isocratic run for next 2.5 min at 100% B. The flow from HPLC column was split into 1:100 and directed into the electrospray ionization source (ESI) of a LTQ linear ion trap MS (ThermoFinnigan, San Jose, CA) controlled with Xcalibur software (v 1.4, ThermoFinnigan, San Jose, CA). The electrospray voltage was set to +5 kV. Nitrogen sheath and auxiliary gas flow was 60 and 20 arbitrary units, respectively. The ion transfer capillary temperature was 350 °C. Single ion monitoring scan spectra were acquired from 366.5 to 371.5 amu and from 404.7 to 409.7 amu at unit mass resolution with maximum injection time set to 200 ms in one micro scan. The range of selected amu values corresponds to $[M+H]^+$ parent unmodified curcumin (369) and monoalkyne curcumin (407), respectively. Based on the relative abundance of curcumin and monoalkyne curcumin peaks, the reaction efficiency was approximately 56%. In the preparatory mode, major split flow from the HPLC system was directed to the Gilson 203B fraction collector set with a collection mode of 0.5 min per tube. Repeated injections of product mixture were carried out to collect monoalkyne curcumin with a retention time of 6.75 min.

Sensitivity and Specificity of Imaging Curcumin Uptake Inside Cells Using Click Chemistry Based Imaging Approach. The human cervical carcinoma cell line (HeLa) was maintained in a culture medium consisting of DMEM supplemented with 10% FBS and 100 mg/L penicillin. HeLa cells (5×10^4 cells/mL) were seeded into culture flasks, grown in a humidified atmosphere of 5% CO_2−95% air at 37 °C. For imaging, cells were cultured on 8 well coverslip bottom culture chambers.

Sensitivity of in situ detection of monoalkyne curcumin and unmodified curcumin in cells was compared using fluorescence imaging. HeLa cells were incubated with monoalkyne curcumin and unmodified curcumin at a concentration of 3.2 μM for 4 h. Both samples were then washed three times with PBS. Cells incubated with monoalkyne curcumin were fixed with 3.7% formaldehyde at 4 °C. After 30 min of fixation, formaldehyde was removed and the cells were washed three times with excess PBS. HeLa cells were then incubated with the click chemistry reaction buffer (0.1 M Tris-Buffer (pH = 8.5) with 0.05% Triton, 10 μM Alexa-488 azide, 1 mM $CuSO_4$, and 50 mM ascorbic acid) for in situ labeling of monoalkyne curcumin with an azide-modified fluorophore for 30 min in the dark, at room temperature. After the click chemistry reaction, the incubation medium was removed and the cells were washed twice with PBS.

Fluorescence signal was measured using an inverted fluorescence microscope (IX71, Olympus Inc., Center Valley, PA). Excitation and emission filters for imaging the intracellular uptake of monoalkyne curcumin were 470/15 nm and 515−550 nm, respectively. Since curcumin has a relatively broad excitation and emission spectrum, the cells incubated with unmodified curcumin were excited at the wavelengths of 380/15 nm and 470/15 nm, respectively. The emission signal was collected using two band-pass emission filters 420−460 nm and 515−550 nm, respectively. Autofluorescence of the control HeLa cells was also measured using fluorescence microscopy with a 380/15 nm band-pass excitation filter and a 420−460 nm band-pass emission filter.

Specificity of the click chemistry reaction for imaging intracellular delivery of monoalkyne curcumin was validated using a negative control. In this control experiment, cells were exposed to Alexa-488 azide dye without prior incubation of cells with monoalkyne curcumin. Both the treatment and control samples were subsequently fixed, stained, and imaged using the procedure described above.

Intracellular Uptake of Monoalkyne Curcumin in 2-d Cell Culture as a Function of Incubation Time and Concentration. HeLa cells were incubated with monoalkyne curcumin at selected concentration levels (ranging from 1.6 to 64 μM) for a specified incubation time (ranging from 0 to 12 h). The cells were subsequently washed three times with excess PBS and fixed with 3.7% formaldehyde at 4 °C. After 30 min fixation, cells were washed with PBS three times and incubated with the click chemistry reaction buffer for 30 min as described in the previous section. The cells were then washed twice with PBS and imaged using an inverted fluorescence microscope (IX71, Olympus Inc.). The excitation and emission band-pass filters were 470/15 nm and 515−550 nm, respectively. The camera exposure time for an individual image was 500 ms.

Characterization of Biological Activity of Monoalkyne Curcumin. Antiproliferative properties of monoalkyne curcumin were characterized using the MTT assay (3-(4,5-dimethylthiazol-2-yl)-2,5-diphenyltetrazolium bromide, a yellow tetrazole) (ATCC, Manassas, VA). HeLa cells cultured in a 24-well plate were incubated with monoalkyne curcumin and unmodified curcumin, respectively, at concentration levels of 16, 32, and 64 μM. These levels of concentration were selected based on the results of prior studies that have evaluated antiproliferative activity of unmodified curcumin.[36] After incubation for 24 h, 10 μL of the MTT reagent was added to each well including the control samples (cells only and cell culture media only), and the plates were incubated for 3 h at 37 °C. After 3 h, 100 μL of the detergent reagent (as supplied with the MTT assay kit) was added to each well of the 24 well-plate. The plate was incubated overnight in the dark at room temperature. The absorbance in each well was measured at 570 nm in a microtiter plate reader including the control samples.

Encapsulation of Monoalkyne Curcumin in DSPE-PEG Micelles. DSPE-PEG-amine was dissolved in methanol to obtain a final concentration of 10 mg/mL. One milliliter of the

dx.doi.org/10.1021/bc4002008 | Bioconjugate Chem. 2014, 25, 32−42

DSPE-PEG-amine solution was mixed with a 50 μL of the monoalkyne curcumin solution prepared in methanol (3.5 mg/mL). The resultant mixture was placed under nitrogen stream for 10 min to evaporate methanol. To this dried mixture, 2 mL of distilled water was added to spontaneously form the DSPE-PEG micelles encapsulating monoalkyne curcumin. The micelle solution was filtered through a 0.22 μm filter prior to incubation with cells.

DSPE-PEG micelles encapsulating curcumin monoalkyne were labeled with Alexa Fluor 647ester (1 mM) in the dark for 1 h, followed by incubation at 4 °C overnight. This reaction approach specifically labels the primary amine attached to the headgroup of PEG molecules with an Alexa-647 ester dye. Fluorescently prelabeled micelle was purified to remove any free dye using column purification (ZebaTM Spin Desalting Column 7K MWCO, Thermo, Rockford, IL).

Particle Size Measurement and Monoalkyne Curcumin Loading. Particle size of monoalkyne curcumin loaded micelles was measured using a dynamic light scattering particle size analyzer (Malvern Nano Series, Malvern Instruments, Inc., Westborough, MA). The setting for the analyzer were material type: oil, particle refractive index = 1.45, dispersant type: water, dispersant refractive index = 1.33, temperature: 25 °C. Particle size measurement was analyzed based on the number average particle size distribution. To measure the loading of monoalkyne curcumin in DSPE-PEG micelles, 100 μL of the micelle solution was incubated with 900 μL DMSO to disrupt the micelles and to extract encapsulated monoalkyne curcumin. The absorbance of the DMSO solution was measured at 425 nm using UV−vis spectrophotometer (Genesys, S10). Monoalkyne curcumin concentration was calculated from the standard curve prepared by varying the concentration of monoalkyne curcumin in DMSO.

Formation of Tissue Phantoms. Tissue phantoms were prepared using the HeLa cells embedded in a collagen matrix. Type I collagen was dissolved in 0.2% acetic acid to 3 mg/mL. To prepare a high density tissue phantom, a suspension of HeLa cells was spun down and resuspended in a small volume of DMEM (Invitrogen, Carlsbad, CA) containing 10% FBS so that there were 1×10^8 cells/mL. The collagen−cell suspension mixture was prepared by mixing concentrated cell suspension with collagen in 2:1 volumetric ratio. 1 M NaOH was gradually added into the mixture to achieve a pH of 7.4. Subsequently, the suspension was pipetted into a 24 mm transwell with a 3.0 μm pore polycarbonate membrane at the bottom (Corning Incorporated, Corning, NY). These transwells were placed in a 24-well plate with 500 μL of DMEM containing 10% FBS in each inserted well. The collagen-cell matrix was allowed to gel at 37 °C for 30 min. After forming the tissue phantom, 40 μL of cell culture media was added on top of the phantom. Tissue phantom were kept in DMEM media containing 10% FBS for approximately 48 h at 37 °C. This incubation time enables formation of a highly dense tissue phantom that mimics both the structural features and optical properties of oral epithelial tissues.[37]

Delivery of Monoalkyne Curcumin Loaded Micelles in 2-d Cell Culture and 3-d Tissue Phantom Models. HeLa cells in culture were incubated with fluorescently labeled DSPE-PEG micelles encapsulating monoalkyne curcumin at a concentration of 32 μM. After an incubation period of 12 h, cells were fixed using 3.7% formaldehyde in PBS at 4 °C. After 30 min of fixation, formaldehyde was removed and the specimens were washed three times with PBS. Samples were incubated with the click chemistry reaction buffer as described earlier.

Fluorescence signal from stained HeLa cells was measured using an inverted fluorescence microscope (IX71, Olympus Inc.). The excitation and emission filters set for imaging monoalkyne curcumin labeled with Alexa-488 azide were 470/15 nm and 515−550 nm, respectively. The excitation and emission filters set for imaging Alexa-647 labeled DSPE-PEG were 630/15 nm and 670−710 nm, respectively.

Labeled DSPE-PEG-amine micelles (labeled with Alexa-647) encapsulating monoalkyne curcumin at a concentration of 32 μM were topically delivered to 3-d tissue phantoms. Tissue phantoms were incubated for 48 h with topically applied micelle solution. After this incubation period, tissue phantoms were transversely sectioned, fixed, and stained with Alexa-488 azide to detect distribution of monoalkyne curcumin in the model tissues using the experimental approaches described above. Fluorescence confocal images (Zeiss LSM 510 confocal microscope) were obtained using a 488 and 633 nm excitation wavelengths, respectively. Corresponding to their excitation wavelengths, the fluorescence emission signals for Alexa-488 azide labeled monoalkyne curcumin and Alexa-647 labeled DSPE-PEG were collected using the BP 520−550 and BP 655−719 emission filters, respectively.

Image Quantification and Analysis. Fluorescence microscopy data was quantified by calculating the mean fluorescence intensity (MFI) of individual cells within selected field of view (FOV) using ImageJ (Public domain, NIH) software. The MFI of individual cells was corrected by subtracting the background fluorescence signal from a region on a chamber coverslip without any cells. The average MFI was calculated by averaging the MFI from all the selected FOVs. Multiple FOVs (typically 9−10 FOVs with approximately 50−80 cells in total) were analyzed from three independent experiments for each of the experimental conditions. The average MFI and standard deviation were calculated for each of the experimental condition. To characterize changes in the intracellular distribution of monoalkyne curcumin as a function of incubation time, the intensity line scans were generated to quantify variation in distribution of monoalkyne curcumin in cells. Line scans were also used for comparing intracellular distribution of monoalkyne curcumin and DSPE-PEG in a 2-d cell culture model.

Percentage colocalization of monoalkyne curcumin and fluorescently prelabeled DSPE-PEG in cells and tissues was measured using the colocalization index function in the MetaMorph software (Molecular Devices, LLC, CA). Briefly, simultaneously acquired fluorescence images of monoalkyne curcumin and prelabeled DSPE-PEG were thresholded to the same conditions prior to performing the colocalization measurements. The colocalization percentage was calculated by measuring the spatial overlap of the pixels in the images corresponding to Alexa-488 azide labeled monoalkyne curcumin and Alexa-647 labeled DSPE-PEG molecules. These measurements were repeated for multiple independent set of images to calculate the mean colocalization index.

Statistical Analysis. Statistical analysis was carried out using Microsoft Excel 2007 (Microsoft Inc., Bellevue, WA) and SAS (version 9.1 SAS Inc., Cary NC). Student's *t* test was used for evaluating statistical significance between the treatments.

dx.doi.org/10.1021/bc4002008 | *Bioconjugate Chem.* 2014, 25, 32−42

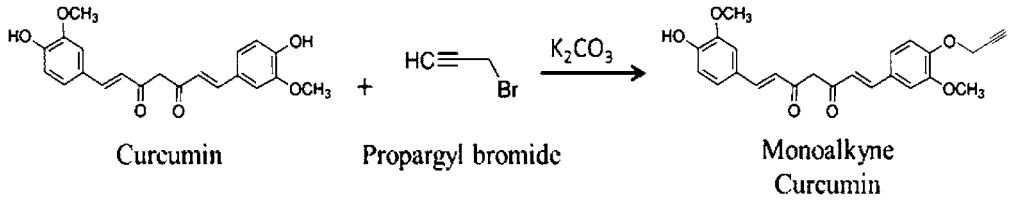

Figure 1. Synthesis of monoalkyne curcumin.

RESULTS

Synthesis and Purification of Monoalkyne Curcumin. Figure 1 outlines the schematic approach for the synthesis of monoalkyne curcumin. After initial purification on a C-18 column, the reaction mixture was analyzed using a LC-MS. The HPLC chromatogram for the purified monoalkyne curcumin is shown in Supporting Information Figure S1. The final concentration of monoalkyne curcumin obtained after HPLC purification was 3.5 mg/mL and the purity of the product was approximately 98%.

Specificity of Imaging Intracellular Uptake of Monoalkyne Curcumin. To demonstrate specificity of the click chemistry based imaging approach for in situ detection of monoalkyne curcumin in cells, control cells (not incubated with monoalkyne curcumin) were stained with Alexa-488 azide using the same experimental procedure as in the case of treated cells. HeLa cells incubated with monoalkyne curcumin showed intense fluorescence after staining with Alexa-488 azide (Figure 2A). In contrast, the control cells (Figure 2B) showed no

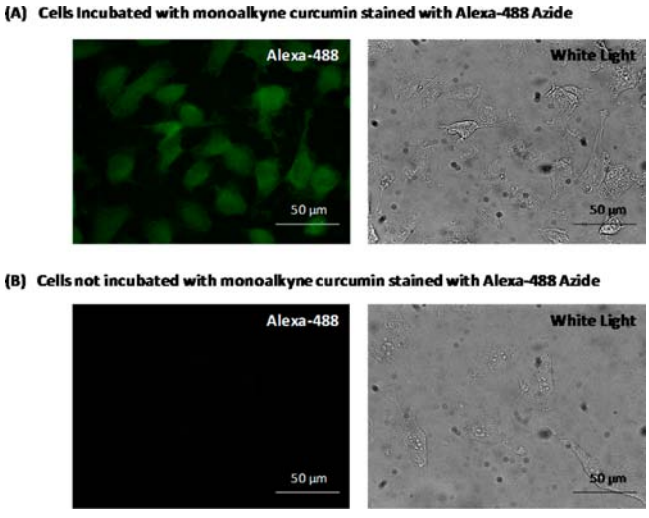

Figure 2. Fluorescence and corresponding white light images of HeLa cells incubated (A) with monoalkyne curcumin at a concentration of 3.2 μM for 4 h and stained with Alexa-488 azide; (B) without monoalkyne curcumin but stained with Alexa-488 azide.

detectable fluorescence signal in HeLa cells when subjected to the same fixation and staining conditions as used for the treated cells (Figure 2A). These results indicate high specificity of the click chemistry reaction for in situ imaging of monoalkyne curcumin in cells. Sensitivity of the click chemistry based imaging approach for in situ detection of curcumin was compared with curcumin autofluorescence based measurement by comparing the MFI of cells incubated with monoalkyne curcumin and unmodified curcumin (Supporting Information Figure S2).

Kinetics of Uptake of Monoalkyne Curcumin in HeLa Cells. Figure 3A shows the results of imaging based measurements to characterize the uptake of monoalkyne curcumin in HeLa cells as a function of incubation time. The MFI for individual cells was quantified as a function of incubation time as described in the Materials and Methods section (Figure 3B). The results show that the uptake of monoalkyne curcumin in cells was detected within 15 min of incubation. Fluorescence intensity measurements corresponding to the uptake of monoalkyne curcumin in cells showed a rapid increase during the first hour of incubation ($p < 0.005$), followed by a relatively slower rate of increase in the MFI during the following 3 h of incubation ($p < 0.05$). The MFI increased marginally during the incubation period between 4 and 8 h and showed a slight decrease during 8−12 h of incubation. In addition to changes in the MFI, a significant change in intracellular distribution of curcumin was also observed as a function of incubation time. To illustrate these differences, representative line scans through selected cells incubated with monoalkyne curcumin for 4 and 8 h are shown in Supporting Information Figure S3.

Intracellular Uptake of Monoalkyne Curcumin as a Function of Concentration. Figure 4A shows the results of imaging measurements to characterize the intracellular uptake of monoalkyne curcumin as a function of concentration of monoalkyne curcumin added to the cell culture media. Imaging data was acquired after 4 h of incubation. This time period was selected based on the results in Figure 3B. The MFI within individual cells as a function of concentration of monoalkyne curcumin is shown in Figure 4B. These imaging results show that the MFI increased with an increase in concentration of monoalkyne curcumin up to 32 μM ($p < 0.005$). Statistical analysis of the MFI values of cells incubated with 32 and 64 μM concentrations of monoalkyne curcumin, respectively, showed no significant difference ($p > 0.005$). Furthermore, changes in the incubation concentration of monoalkyne curcumin did not influence the intracellular distribution of fluorescent signal representing distribution of monoalkyne curcumin in cells.

Characterization of Antiproliferative Activity of Curcumin-Monoalkyne. Antiproliferative activity of curcumin and monoalkyne curcumin was compared to demonstrate that derivatization of curcumin to include a monoalkyne tag did not cause significant changes in the functional properties of curcumin. Antiproliferative activity of monoalkyne curcumin was measured based on its ability to induce cell death in cancer cells. This antiproliferative activity of curcumin in cancer cell lines has been demonstrated in prior studies.[38−40] Figure 5 compares reduction in viability of HeLa cells treated with monoalkyne curcumin or unmodified curcumin using the MTT assay. Compared to the control cells (HeLa cells cultured in medium), curcumin or monoalkyne curcumin treated cells show significant reduction in cell viability after 24 h of incubation ($p < 0.005$). The cell viability decreased with an

dx.doi.org/10.1021/bc4002008 | Bioconjugate Chem. 2014, 25, 32−42

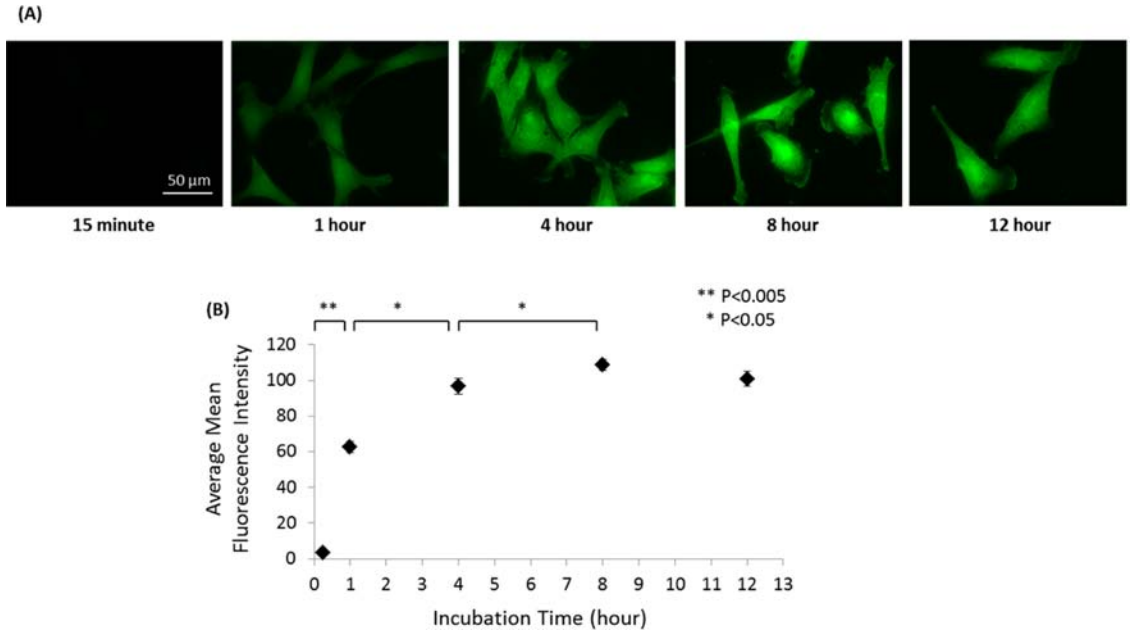

Figure 3. Imaging uptake of monoalkyne curcumin in HeLa cells as a function of incubation time. Fluorescence images of HeLa cells incubated with monoalkyne curcumin at a concentration of 32 μM and stained with Alexa-488 azide. (A) Fluorescence images show change in fluorescence intensity as a function of incubation time (over 12 h). (B) Quantification of average mean fluorescence signal intensity of HeLa cells incubated with monoalkyne curcumin as a function of incubation time.

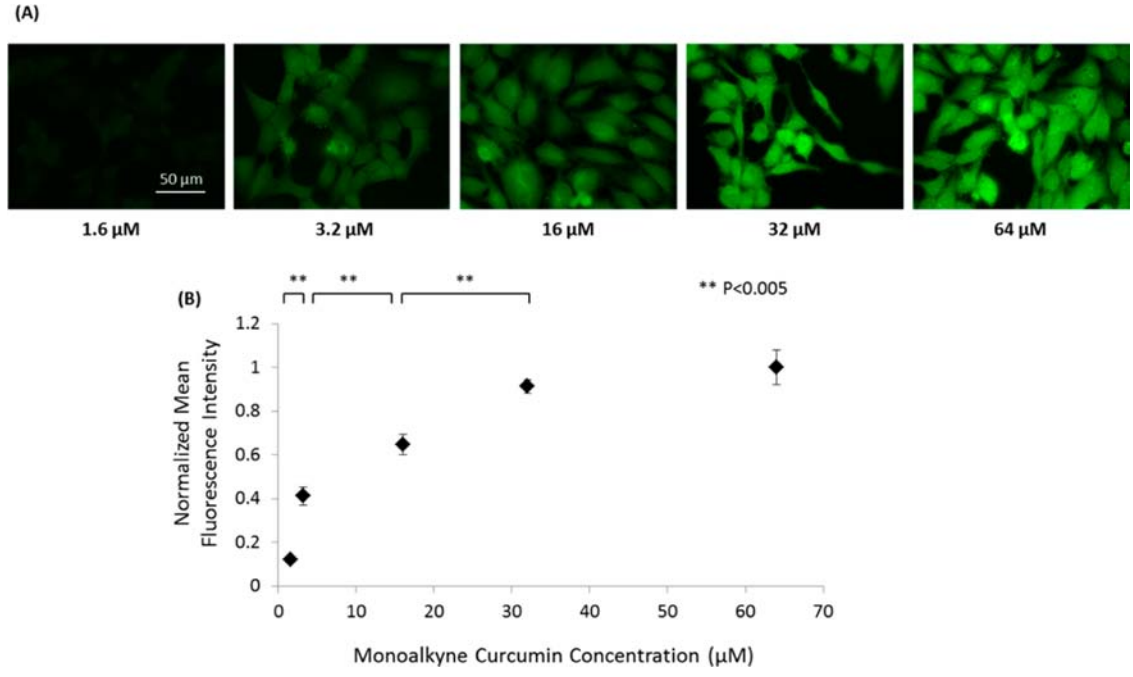

Figure 4. Intracellular uptake of monoalkyne curcumin in 2-d cell culture as a function of concentration. HeLa cells were incubated with monoalkyne curcumin at the selected concentrations for 4 h. (A) Fluorescence images show increase in fluorescence intensity with increasing concentration of monoalkyne curcumin. (B) Quantification of normalized mean fluorescence signal intensity of HeLa cells as a function of monoalkyne curcumin concentration.

increase in concentration of curcumin or monoalkyne curcumin (ranging between 16 and 64 μM). Statistical analysis also showed that there was no significant difference ($p > 0.05$) in the antiproliferative activity of curcumin and monoalkyne curcumin in the concentration range of 16 μM to 64 μM. These results indicate that derivatization of curcumin to include a monoalkyne tag did not significantly change the antiproliferative property of curcumin.

Fate of Encapsulated Curcumin and Its Encapsulating Matrix after Topical Delivery in 2-d Cell Culture Model. To demonstrate simultaneous imaging of both the carrier (encapsulating material) and the encapsulant molecules in cells and tissues, monoalkyne curcumin was encapsulated in DSPE−PEG micelles. Figure 6A shows the schematic design of the micelle formulation. The particle size of DSPE-PEG micelles encapsulating monoalkyne curcumin and the concentration of

dx.doi.org/10.1021/bc4002008 | *Bioconjugate Chem.* 2014, 25, 32−42

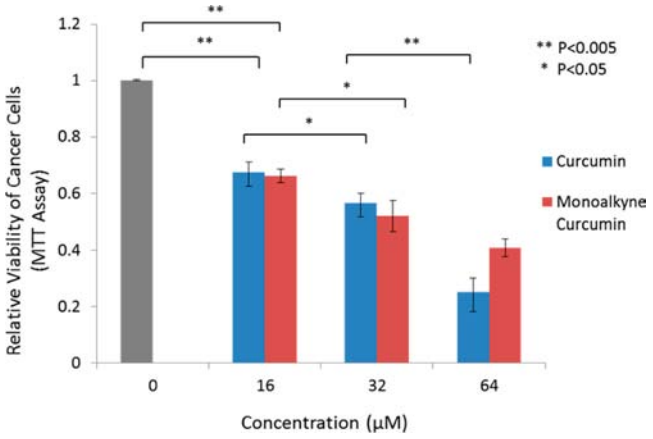

Figure 5. Characterization of antiproliferative properties of monoalkyne curcumin. The MTT assay was used for evaluating changes in viability of HeLa cells after incubation with monoalkyne curcumin and curcumin, respectively, at the selected concentrations for 24 h.

monoalkyne curcumin in micelles was measured as described in the Materials and Methods section. The mean particle diameter based on dynamic light scattering measurements of DSPE-PEG micelles was 14.5 ± 0.3 nm. The monoalkyne curcumin concentration in the micelles was found to be 66.7 μg/mL. Based on the amount of monoalkyne curcumin originally added in the DSPE-PEG-amine solution during the synthesis process, the loading efficiency of curcumin in DSPE-PEG micelles was calculated to be 76%.

To simultaneously image the intracellular distribution of DSPE-PEG and encapsulated curcumin, the micelles were prelabeled with an Alexa-647 ester dye and monoalkyne curcumin was detected using a click chemistry reaction with an Alexa-488 azide as described in the Materials and Methods section. Figure 6B shows the results of simultaneous imaging of both monoalkyne curcumin (green) and DSPG-PEG (red). These results indicate that curcumin molecules have a distinct intracellular fate compared to the encapsulating matrix of DSPE-PEG. To characterize these differences in intracellular distribution, a normalized intensity line scan was generated across a representative cell (Figure 6C). The results show that, although the micelles were delivered in the cells, the fluorescent signal from the DSPE-PEG was localized in the cytoplasmic compartment of cells, while the monoalkyne curcumin was distributed throughout the cells including both the cytoplasmic and the nuclear compartments.

Fate of Encapsulated Curcumin and Its Encapsulating Matrix after Topical Delivery in 3-d Tissue Phantom Models. Figure 7 shows the results of simultaneous imaging of DSPE−PEG and monoalkyne curcumin in a transverse tissue section, following topical delivery of monoalkyne curcumin encapsulated in micelles to a 3-d tissue phantom. Imaging of transverse sections of a tissue model was performed to map the uniformity of delivery of monoalkyne curcumin and micelles along the depth of a 3-d tissue phantom. Results of the imaging measurements show that monoalkyne curcumin initially encapsulated in micelles was effectively delivered throughout the depth of the tissue in a 48 h incubation period. The results also show that there were significant differences in the localization of monoalkyne curcumin and DSPE-PEG within a tissue section. A significant fraction of DSPE-PEG was entrapped in the extracellular space, while monoalkyne curcumin was predominantly located inside cells and concentrated in the nuclear compartment of cells. Quantitative image analysis shows that the colocalization area of the monoalkyne curcumin and DSPE-PEG inside cells was

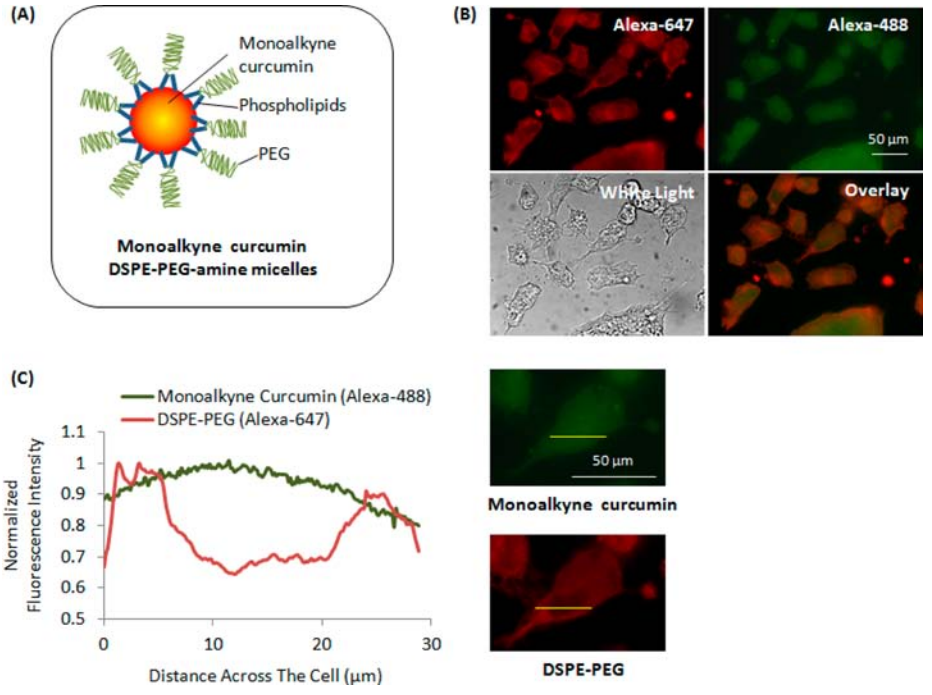

Figure 6. (A) Schematic illustration of the design of DSPE-PEG-amine micelles encapsulating monoalkyne curcumin. (B) Simultaneous imaging of the intracellular distribution of DSPE-PEG and monoalkyne curcumin in a 2-d cell culture model. DSPE-PEG-amine micelles were labeled with Alexa-647 ester (red), while monoalkyne curcumin was labeled with Alexa-488 azide (green). (C) Fluorescence line scan to map spatial distribution of monoalkyne curcumin and DSPE-PEG in HeLa cells. A zoomed-in image of the representative cell corresponding to the line scan is shown.

dx.doi.org/10.1021/bc4002008 | *Bioconjugate Chem.* 2014, 25, 32−42

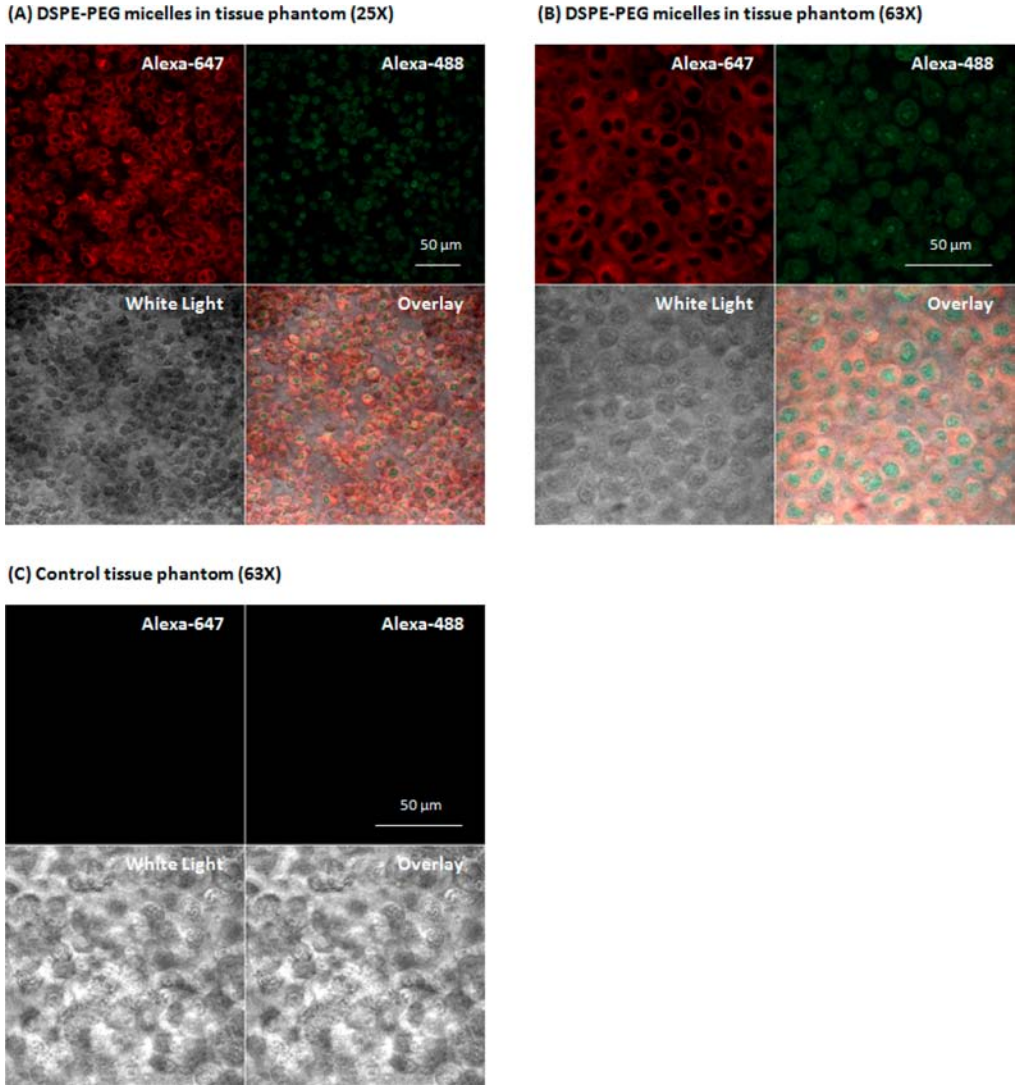

Figure 7. Simultaneous imaging of the intratissue distribution of DSPE-PEG (labeled with Alexa-647) and monoalkyne curcumin (labeled with Alexa-488) in a 3-d tissue phantom. Tissue phantoms were topically applied of micelle solution. Confocal fluorescence and corresponding white light images of the transverse section of tissue phantom at (A) 25× and (B) 63× magnifications. (C) A control phantom was not incubated with DSEP-PEG micelle encapsulating monoalkyne curcumin and imaged with 63× magnification.

approximately 65% (±4.5%) (Figure 7A,B). These results indicate that, in the tissue environment, a significant fraction of micelles was disrupted prior to intracellular delivery of encapsulated molecules. Changes in the micellar structure may be induced by interactions of the micelles with ECM (extracellular matrix) molecules such as collagen. Figure 7C shows the results of imaging measurements of a transverse tissue section of a control tissue phantom not incubated with monoalkyne curcumin but fixed and stained under the same conditions as the tissue phantom incubated with DSPE-PEG micelles encapsulating monoalkyne curcumin (Figure 7A,B). The imaging results show no significant background staining in the control tissue phantom sections. The low background signal from the control tissue phantom further demonstrates the high specificity of detecting intracellular curcumin in a 3-d tissue environment using the click chemistry based imaging approach. Overall, the results of these measurements in a tissue model demonstrate that simultaneous imaging of the fate of encapsulation matrix and the encapsulant provides fundamental insight into the design of delivery systems.

DISCUSSION

Click Chemistry Approach for Molecular Tagging of Curcumin. In this study, a monoalkyne derivative of curcumin was synthesized for imaging intracellular uptake of curcumin. This click chemistry based imaging approach was selected because monoalkyne modification of curcumin molecule introduces a relatively smaller change (38 Da) in the molecular weight of the native curcumin molecule as compared to conjugation with other conventional fluorescent dyes.[41] Additionally, the monoalkyne tag is highly stable and cannot be metabolized by the intracellular enzymatic processes.[24−26,42] The results of this study also highlight that the modified form of curcumin maintains its biological properties as exemplified by induction of apoptosis in cancer cells (Figure 5), a property of curcumin that has been well characterized in several prior studies.[23,38,43]

Sensitivity and Specificity of Imaging Curcumin Uptake in Cells and Tissues. A few studies have previously imaged curcumin uptake in cells based on fluorescence properties of unmodified curcumin.[13,14] The results of this

dx.doi.org/10.1021/bc4002008 | Bioconjugate Chem. 2014, 25, 32−42

study highlight that the image contrast obtained using the click chemistry based staining of monoalkyne curcumin is at least 2 orders of magnitude higher than the image contrast obtained based on autofluorescence properties of curcumin (Figure S2), thus improving sensitivity of the imaging measurements. Due to a significant spectral overlap between the fluorescence properties of curcumin and the autofluorescence properties of tissues, it is expected that sensitivity of detecting unmodified curcumin in tissues will be limited.[16] In addition, comparison of imaging measurements between cells and tissues incubated with or without monoalkyne curcumin demonstrates high specificity and efficiency of imaging monoalkyne curcumin delivery in cellular and tissue environments using click chemistry (Figures 2A,B and 7).

Simultaneous Imaging of the Fate of Encapsulated Bioactive and Its Carrier. Due to limited solubility of curcumin in aqueous environments, curcumin molecules are often encapsulated in micelles, liposomes, and nanoparticles for diverse biomedical applications. Prior studies have highlighted the role of encapsulated structures in improving delivery of curcumin in both in vitro and in vivo models.[8,13,44] Despite significant potential benefits of encapsulation systems, there is limited understanding of the intracellular and intratissue fate of both the encapsulating matrix and the bioactive encapsulant.

Simultaneous imaging of monoalkyne curcumin and the DSPE-PEG micelles showed distinct localization of DSPE−PEG and curcumin in both cells and tissue models. Curcumin showed a strong affinity to partition in the nuclear compartment of the cells even though the encapsulating matrix was predominantly localized in the cytoplasm and extracellular space (Figures 6B,C and 7). This result is supported by the evidence that curcumin has affinity to bind DNA molecules based on hydrogen bonding interactions with the minor groove in AT-rich regions.[45] These results are unique because the prior studies performed to map the fate of nanoscale carriers and the encapsulated molecules are predominantly focused on using fluorescent dyes as model encapsulants.[46,47] Since the fluorescent dyes may not have any specific molecular targets, their localization may not be representative of bioactive molecules that can specifically interact with the molecular targets in cells. A distinct localization of DSPE-PEG and curcumin monoalkyne suggests that structural changes in micelles take place prior to intracellular delivery of monoalkyne curcumin in a tissue model and highlights the need for real time imaging of dynamics of colloidal nanocarriers in a tissue environment. It is important to note that the tissue phantom is a relatively simplified model of a tissue. It is expected that the presence of lipids and other biopolymers in addition to collagen in a tissue matrix may significantly influence the structural dynamics of colloidal carriers. The results of this study highlight the need for real time characterization of the dynamics of colloidal assemblies in cellular and tissue environment.

In addition, it is known that curcumin molecules can bind a diverse class of inflammatory proteins such as TNF-alpha, multiple enzymes such as MMPs, proteasome and structural proteins such as tubulin.[45] Most of these binding measurements are based on biochemical interactions in vitro with limited evidence in cells. The approach developed in this study can be combined with fluorescently tagged proteins and enzymes to understand interactions of curcumin in cells and in tissues. These measurements can complement the conventional biochemical analysis in which curcumin binding is predominantly characterized using cell and tissue lysates. The unique advantage of imaging based characterization in this study can be used to determine the partitioning of curcumin in distinct compartments of cells and tissues and its in situ association with target molecules in diverse physiological states including inflammation and cancer. These imaging measurements will complement the biochemical analysis to measure the diverse functions of curcumin and its derivatives and enable fundamental understanding of the biological activity of curcumin in diverse patho-physiologies. This understanding is critical to enable clinical translation of these bioactives for both prevention and treatment of diseases.

■ CONCLUSIONS

A novel optical imaging approach to map intracellular and intratissue distribution of small bioactive molecules is discussed. The novel approach is based on a monoalkyne derivative of curcumin that can be conjugated with Alexa-488 azide after its delivery in cells and tissue. Using the imaging approach, changes in the uptake of monoalkyne curcumin as a function of concentration and incubation time in cancer cells were measured and quantified with high sensitivity and specificity. Compared with unmodified curcumin, monoalkyne curcumin showed similar biological activity in inducing cell death in cancer cells. A novel approach for simultaneous imaging of both the nanoscale DSPE-PEG micelle carriers and encapsulated curcumin in cell and tissue model systems is also discussed. Results of imaging measurements showed a distinct distribution of DSPE-PEG and monoalkyne curcumin in cells and tissues. Overall, this study demonstrates a novel approach to image spatial distribution of bioactive compounds in cells and enables simultaneous imaging of colloidal nanocarriers and encapsulated bioactives in both cells and tissues. The results of this study have significant impact on characterization of delivery of bioactives using diverse encapsulation systems as well as fundamental understanding of interactions of bioactive compounds with cellular and tissue targets.

■ ASSOCIATED CONTENT

Ⓢ Supporting Information

Additional data of purification and characterization of monoalkyne curcumin is presented (Figure S1). Sensitivity of imaging intracellular uptake of monoalkyne curcumin (Figure S2), and intracellular localization of monoalkyne curcumin in HeLa cells (Figure S3) is also characterized. This material is available free of charge via the Internet at http://pubs.acs.org.

■ AUTHOR INFORMATION

Corresponding Author

*Phone: 530-752-6208. E-mail: nnitin@ucdavis.edu.

Notes

The authors declare no competing financial interest.

■ ACKNOWLEDGMENTS

We acknowledge the funding from the NSF-CAPPS for supporting the synthesis and characterization of monoalkyne curcumin. We also acknowledge the technical support from Dr. Timothy Wade from Drexel University for the acquisition of NMR spectra.

REFERENCES

(1) Birt, D. F., Hendrich, S., and Wang, W. Q. (2001) Dietary agents in cancer prevention: flavonoids and isoflavonoids. *Pharmacol. Ther. 90*, 157−177.

(2) Evans, D. A., Hirsch, J. B., and Dushenkov, S. (2006) Phenolics, inflammation and nutrigenomics. *J. Sci. Food Agric. 86*, 2503−2509.

(3) Kim, Y. S., Young, M. R., Bobe, G., Colburn, N. H., and Milner, J. A. (2009) Bioactive food components, inflammatory targets, and cancer prevention. *Cancer Prev. Res. 2*, 200−208.

(4) Milner, J. A. (2008) Nutrition and cancer: Essential elements for a roadmap. *Cancer Lett. 269*, 189−198.

(5) Vanamala, J., Tarver, C. C., and Murano, P. S. (2008) Obesity-enhanced colon cancer: functional food compounds and their mechanisms of action. *Curr. Cancer Drug Targets 8*, 611−633.

(6) Fathi, M., Mozafari, M. R., and Mohebbi, M. (2012) Nanoencapsulation of food ingredients using lipid based delivery systems. *Trends Food Sci. Technol. 23*, 13−27.

(7) Sagalowicz, L., and Leser, M. E. (2010) Delivery systems for liquid food products. *Curr. Opin. Colloid Interface Sci. 15*, 61−72.

(8) Siddiqui, I. A., Adhami, V. M., Ahmad, N., and Mukhtar, H. (2010) Nanochemoprevention: sustained release of bioactive food components for cancer prevention. *Nutr. Cancer 62*, 883−890.

(9) Onwulata, C. I. (2012) Encapsulation of new active ingredients. *Annu. Rev. Food Sci. Technol. 3*, 183−202.

(10) Li, X. Y., Li, T. H., Guo, J. S., Wei, Y., Jing, X. B., Chen, X. S., and Huang, Y. B. (2012) PEGylation of bovine serum albumin using click chemistry for the application as drug carriers. *Biotechnol. Prog. 28*, 856−861.

(11) Fang, M., Jin, Y., Bao, W., Gao, H., Xu, M., Wang, D., Wang, X., Yao, P., and Liu, L. (2012) In vitro characterization and in vivo evaluation of nanostructured lipid curcumin carriers for intragastric administration. *Int. J. Nanomed. 7*, 5395−404.

(12) Khalil, N. M., Nascimento, T. C., Casa, D. M., Dalmolin, L. F., Mattos, A. C., Hoss, I., Romano, M. A., and Mainardes, R. M. (2012) Pharmacokinetics of curcumin-loaded PLGA and PLGA-PEG blend nanoparticles after oral administration in rats. *Colloids Surf., B 28*, 353−360.

(13) Kunwar, A., Barik, A., Pandey, R., and Priyadarsini, K. I. (2006) Transport of liposomal and albumin loaded curcumin to living cells: an absorption and fluorescence spectroscopic study. *Biochim. Biophys. Acta 10*, 8.

(14) Sahu, A., Kasoju, N., and Bora, U. (2008) Fluorescence study of the curcumin-casein micelle complexation and its application as a drug nanocarrier to cancer cells. *Biomacromolecules 9*, 2905−2912.

(15) Bottiroli, G., and Croce, A. C. (2004) Autofluorescence spectroscopy of cells and tissues as a tool for biomedical diagnosis. *Photochem. Photobiol. Sci. 3*, 189−210.

(16) Pavlova, I., Williams, M., El-Naggar, A., Richards-Kortum, R., and Gillenwater, A. (2008) Understanding the biological basis of autofluorescence imaging for oral cancer detection: high-resolution fluorescence microscopy in viable tissue. *Clin. Cancer Res. 14*, 2396−404.

(17) Cheng, Z., Levi, J., Xiong, Z., Gheysens, O., Keren, S., Chen, X., and Gambhir, S. S. (2006) Near-infrared fluorescent deoxyglucose analogue for tumor optical imaging in cell culture and living mice. *Bioconjugate Chem. 17*, 662−9.

(18) Lee, I., Yang, J., Lee, J. H., and Choe, Y. S. (2011) Synthesis and evaluation of 1-(4-[(1)(8)F]fluoroethyl)-7-(4′-methyl)curcumin with improved brain permeability for beta-amyloid plaque imaging. *Bioorg. Med. Chem. Lett. 21*, 5765−9.

(19) Ryu, E. K., Choe, Y. S., Lee, K. H., Choi, Y., and Kim, B. T. (2006) Curcumin and dehydrozingerone derivatives: synthesis, radiolabeling, and evaluation for beta-amyloid plaque imaging. *J. Med. Chem. 49*, 6111−9.

(20) Nitin, N., Carlson, A. L., Muldoon, T., El-Naggar, A. K., Gillenwater, A., and Richards-Kortum, R. (2009) Molecular imaging of glucose uptake in oral neoplasia following topical application of fluorescently labeled deoxy-glucose. *Int. J. Cancer 124*, 2634−42.

(21) Nair, H. B., Sung, B., Yadav, V. R., Kannappan, R., Chaturvedi, M. M., and Aggarwal, B. B. (2010) Delivery of antiinflammatory nutraceuticals by nanoparticles for the prevention and treatment of cancer. *Biochem. Pharmacol. 80*, 1833−43.

(22) Visioli, F., De La Lastra, C. A., Andres-Lacueva, C., Aviram, M., Calhau, C., Cassano, A., D'Archivio, M., Faria, A., Fave, G., Fogliano, V., Llorach, R., Vitaglione, P., Zoratti, M., and Edeas, M. (2011) Polyphenols and human health: a prospectus. *Crit. Rev. Food Sci. Nutr. 51*, 524−46.

(23) Weng, C. J., and Yen, G. C. (2012) Chemopreventive effects of dietary phytochemicals against cancer invasion and metastasis: phenolic acids, monophenol, polyphenol, and their derivatives. *Cancer Treat. Rev. 38*, 76−87.

(24) Hsu, T. L., Hanson, S. R., Kishikawa, K., Wang, S. K., Sawa, M., and Wong, C. H. (2007) Alkynyl sugar analogs for the labeling and visualization of glycoconjugates in cells. *Proc. Natl. Acad. Sci. U. S. A. 104*, 2614−2619.

(25) Chang, P. V., Chen, X., Smyrniotis, C., Xenakis, A., Hu, T. S., Bertozzi, C. R., and Wu, P. (2009) Metabolic labeling of sialic acids in living animals with alkynyl sugars. *Angew. Chem., Int. Ed. 48*, 4030−4033.

(26) Yap, M. C., Kostiuk, M. A., Martin, D. D. O., Perinpanayagam, M. A., Hak, P. G., Siddam, A., Majjigapu, J. R., Rajaiah, G., Keller, B. O., Prescher, J. A., Wu, P., Bertozzi, C. R., Falck, J. R., and Berthiaume, L. G. (2010) Rapid and selective detection of fatty acylated proteins using omega-alkynyl-fatty acids and click chemistry. *J. Lipid Res. 51*, 1566−1580.

(27) Shaikh, J., Ankola, D. D., Beniwal, V., Singh, D., and Kumar, M. N. V. R. (2009) Nanoparticle encapsulation improves oral bioavailability of curcumin by at least 9-fold when compared to curcumin administered with piperine as absorption enhancer. *Eur. J. Pharm. Sci. 37*, 223−230.

(28) Yang, R. L., Zhang, S. A., Kong, D. L., Gao, X. L., Zhao, Y. J., and Wang, Z. (2012) Biodegradable polymer-curcumin conjugate micelles enhance the loading and delivery of low-potency curcumin. *Pharm. Res. 29*, 3512−3525.

(29) Mishra, B., Patel, B. B., and Tiwari, S. (2010) Colloidal nanocarriers: a review on formulation technology, types and applications toward targeted drug delivery. *J. Nanomed. Nanotechnol. 6*, 9−24.

(30) Gaucher, G., Dufresne, M. H., Sant, V. P., Kang, N., Maysinger, D., and Leroux, J. C. (2005) Block copolymer micelles: preparation, characterization and application in drug delivery. *J. Controlled Release 109*, 169−188.

(31) Liaw, J., Chang, S. F., and Hsiao, F. C. (2001) In vivo gene delivery into ocular tissues by eye drops of poly(ethylene oxide)-poly(propylene oxide)-poly(efhylene oxide) (PEO-PPO-PEO) polymeric micelles. *Gene Ther. 8*, 999−1004.

(32) Torchilin, V. P. (2004) Targeted polymeric micelles for delivery of poorly soluble drugs. *Cell. Mol. Life Sci. 61*, 2549−2559.

(33) Chen, H., Kim, S., He, W., Wang, H., Low, P. S., Park, K., and Cheng, J. X. (2008) Fast release of lipophilic agents from circulating PEG-PDLLA micelles revealed by in vivo forster resonance energy transfer imaging. *Langmuir 24*, 5213−7.

(34) Chen, H., Kim, S., Li, L., Wang, S., Park, K., and Cheng, J. X. (2008) Release of hydrophobic molecules from polymer micelles into cell membranes revealed by Forster resonance energy transfer imaging. *Proc. Natl. Acad. Sci. U. S. A. 105*, 6596−601.

(35) Shi, W., Dolai, S., Rizk, S., Hussain, A., Tariq, H., Averick, S., L'Amoreaux, W., El Ldrissi, A., Banerjee, P., and Raja, K. (2007) Synthesis of monofunctional curcumin derivatives, clicked curcumin dimer, and a PAMAM dendrimer curcumin conjugate for therapeutic applications. *Org. Lett. 9*, 5461−5464.

(36) Anuchapreeda, S., Leechanachai, P., Smith, M. M., Ambudkar, S. V., and Limtrakul, P. (2002) Modulation of P-glycoprotein expression and function by curcumin in multidrug-resistant human KB cells. *Biochem. Pharmacol. 64*, 573−582.

(37) Sokolov, K., Galvan, J., Myakov, A., Lacy, A., Lotan, R., and Richards-Kortum, R. (2002) Realistic three-dimensional epithelial tissue phantoms for biomedical optics. *J. Biomed. Opt. 7*, 148−156.
(38) Anand, P., Thomas, S. G., Kunnumakkara, A. B., Sundaram, C., Harikumar, K. B., Sung, B., Tharakan, S. T., Misra, K., Priyadarsini, I. K., Rajasekharan, K. N., and Aggarwal, B. B. (2008) Biological activities of curcumin and its analogues (Congeners) made by man and Mother Nature. *Biochem. Pharmacol. 76*, 1590−611.
(39) Gupta, S. C., Kim, J. H., Prasad, S., and Aggarwal, B. B. (2010) Regulation of survival, proliferation, invasion, angiogenesis, and metastasis of tumor cells through modulation of inflammatory pathways by nutraceuticals. *Cancer Metastasis Rev. 29*, 405−34.
(40) Kunnumakkara, A. B., Anand, P., and Aggarwal, B. B. (2008) Curcumin inhibits proliferation, invasion, angiogenesis and metastasis of different cancers through interaction with multiple cell signaling proteins. *Cancer Lett. 269*, 199−225.
(41) Ouberai, M., Dumy, P., Chierici, S., and Garcia, J. (2009) Synthesis and biological evaluation of clicked curcumin and clicked KLVFFA conjugates as inhibitors of beta-amyloid fibril formation. *Bioconjugate Chem. 20*, 2123−32.
(42) Hong, V., Steinmetz, N. F., Manchester, M., and Finn, M. G. (2010) Labeling live cells by copper-catalyzed alkyne-azide click chemistry. *Bioconjugate Chem. 21*, 1912−1916.
(43) Reuter, S., Eifes, S., Dicato, M., Aggarwal, B. B., and Diederich, M. (2008) Modulation of anti-apoptotic and survival pathways by curcumin as a strategy to induce apoptosis in cancer cells. *Biochem. Pharmacol. 76*, 1340−51.
(44) Bansal, S. S., Goel, M., Aqil, F., Vadhanam, M. V., and Gupta, R. C. (2011) Advanced drug delivery systems of curcumin for cancer chemoprevention. *Cancer Prev. Res. 4*, 1158−71.
(45) Gupta, S. C., Prasad, S., Kim, J. H., Patchva, S., Webb, L. J., Priyadarsini, I. K., and Aggarwal, B. B. (2011) Multitargeting by curcumin as revealed by molecular interaction studies. *Nat. Prod. Rep. 28*, 1937−55.
(46) Torchilin, V. P. (2005) Fluorescence microscopy to follow the targeting of liposomes and micelles to cells and their intracellular fate. *Adv. Drug Delivery Rev. 57*, 95−109.
(47) Chen, H. T., Kim, S. W., Li, L., Wang, S. Y., Park, K., and Cheng, J. X. (2008) Release of hydrophobic molecules from polymer micelles into cell membranes revealed by Forster resonance energy transfer imaging. *Proc. Natl. Acad. Sci. U. S. A. 105*, 6596−6601.